Eur. Phys. J. Appl. Phys. **39**, 267–274 (2007)
DOI: 10.1051/epjap:2007110

THE EUROPEAN PHYSICAL JOURNAL APPLIED PHYSICS

Influence of the disorder on solute dispersion in a flow channel

V.J. Charette[1], E. Evangelista[1], R. Chertcoff[1], H. Auradou[2], J.P. Hulin[2,a], and I. Ippolito[1]

[1] Grupo de Medios Porosos, Facultad de Ingeniería, Universidad de Buenos Aires, Paseo Colón 850, 1063 Buenos Aires, Argentina
[2] Laboratoire Fluides, Automatique et Systèmes Thermiques, UMR No. 7608, CNRS, Universités Paris 6 et 11, Bâtiment 502, Campus Paris Sud, 91405 Orsay Cedex, France

Received: 9 May 2007 / Accepted: 12 June 2007
Published online: 12 July 2007 –

Abstract. Solute dispersion is studied experimentally in periodic or disordered arrays of beads in a capillary tube. Dispersion is measured from light absorption variations near the outlet following a steplike injection of dye at the inlet. Visualizations using dye and pure glycerol are also performed in similar geometries. Taylor dispersion is dominant both in an empty tube and for a periodic array of beads: the dispersivity l_d increases with the Péclet number Pe respectively as Pe and $Pe^{0.82}$ and is larger by a factor of 8 in the second case. In a disordered packing of smaller beads (1/3 of the tube diameter) geometrical dispersion associated to the disorder of the flow field is dominant with a constant value of l_d reached at high Péclet numbers. The minimum dispersivity is slightly higher than in homogeneous nonconsolidated packings of small grains, likely due to wall effects. In a weakly disordered packing with the same beads as in the periodic configuration, l_d is up to 20 times lower than in the latter and varies as Pe^{γ} with $\gamma = 0.5$ or $=0.69$ (depending on the fluid viscosity). A simple model accounting for this latter result is suggested.

PACS. 47.56.+r Flows through porous media – 05.60.Cd Classical transport

1 Introduction

1.1 Objectives of the paper

Tracer and solute dispersion in fluid flows is a widespread process in science and engineering. It is encountered in many applications to analytical chemistry and hydrology as well as environmental, civil and petroleum engineering [1–4]. Understanding dispersion is also important fundamentally, due to its relation with statistical physics [5]. In simple systems with correlation lengths of the velocities of solute particles small compared to the sample size, the variation in the flow direction x of the concentration C of a passive solute (averaged in the other directions) satisfies the convection-diffusion equation (1)

$$\frac{\partial C}{\partial t} + U\,\frac{\partial C}{\partial x} = D\,\frac{\partial^2 C}{\partial x^2}. \qquad (1)$$

Here, U is the flow velocity and D is the longitudinal macroscopic dispersion coefficient. Longitudinal molecular diffusion has a large direct influence on D only if the Péclet number:

$$Pe = \frac{U\ell}{D_m} \qquad (2)$$

is less than 1 (ℓ is a characteristic length of the flow field and D_m is the molecular diffusion coefficient). We are interested here only in the opposite limit $Pe > 1$ for which, generally, $D \gg D_m$. The variation of D with Pe depends then on the structure of the flow field: variation laws may range from $D \propto Pe$ for geometrical dispersion in homogeneous random porous media to $D \propto Pe^2$ for Taylor dispersion in capillary tubes (these mechanisms are discussed in the next Sect. 1.2).

In other systems, non trivial variations of D with exponents intermediate between 1 and 2 have been observed or predicted. Examples are networks of channels similar to those encountered in microfluidics [6,7] and fractures with rough walls [8–11].

The objective of the present work is to suggest explanations for these latter behaviours: more specifically, we seek to demonstrate on simple model systems the transition between Taylor and geometrical dispersion as the disorder of the flow channels increases. Practically, the dispersion of dye is analyzed in flows through long transparent capillary tubes packed with spherical beads.

Different ordered and disordered layouts and different bead to tube diameter ratios are considered: depending on these parameters, a variety of dispersion regimes is observed ranging from geometrical to Taylor dispersion and including intermediate regimes.

1.2 Key dispersion mechanisms

Solute dispersion results from the combined effects of molecular diffusion and of the heterogeneity of fluid

[a] e-mail: hulin@fast.u-psud.fr

velocities both across and/or along streamlines. At large Péclet numbers Pe, longitudinal molecular diffusion parallel to the flow is negligible but transverse diffusion may retain a significant influence by inducing solute exchange between streamlines with different velocities.

A first limiting case is geometrical dispersion encountered in simple porous media such as macroscopically homogeneous random packings of beads. In this case, the magnitude and orientation of the local flow velocity display random variations with a correlation length of the order of the bead diameter d [12,15] while the stream tubes get frequently split. The path of the solute particles can then be viewed as a sequence of random steps, each with a duration $\tau \sim d/U$, superimposed on a drift at the mean velocity $\mathbf{U}$: the corresponding dispersion coefficient is $D \simeq d^2/\tau \sim Ud$ and the dispersivity is $l_d = D/U \sim d$. As a result, the ratio D/D_m should satisfy:

$$\frac{D}{D_m} \sim Pe \tag{3}$$

(the characteristic length scale ℓ is taken equal to d in Eq. (2)). Experimentally, for an homogeneous packing of beads with a narrow distribution of the diameter d, the dispersivity l_d first reaches a minimum value $l_d \simeq 0.6\,d$ for $Pe \simeq 10$, increases then approximately as $Pe^{0.2}$ and becomes constant for $Pe \geq 1000$ with $l_d \simeq 2d$ [16]. These deviations from the expected law $l_d \simeq cst.$ may result from different mechanisms, often predicting logarithmic corrections to the value of l_d: examples of such effects are the influence of mass boundary layers near the pore walls [17–19], stagnation points [20] or slow flow channels [21].

In the second limiting case of Taylor dispersion in a capillary tube of diameter a [22,23], the flow field is a deterministic Poiseuille parallel flow profile. The velocity difference between the wall and axis of the tube stretches the solute front and creates radial concentration gradients which are balanced by transverse molecular diffusion over the tube section: the corresponding diffusion time $\tau \sim a^2/D_m$ represents the characteristic time for the decorrelation of the solute velocity. The longitudinal dispersion coefficient $D \sim U^2\tau$ scales therefore as $D/D_m \propto Pe^2$ with $Pe = Ua/D_m$ (taking this time $\ell = a$ in Eq. (2)). More quantitatively, and for arbitrary values of Pe, one has [23]:

$$\frac{D}{D_m} = 1 + \frac{Pe^2}{192}, \tag{4}$$

or, equivalently:

$$\frac{l_d}{a} = \frac{1}{Pe} + \frac{Pe}{192}. \tag{5}$$

The respective additional terms 1 and $1/Pe$ correspond to longitudinal molecular diffusion and, as mentioned above, are only significant for $Pe < 1$. The same expression is valid for flow between two parallel planes, replacing the coefficient 192 by 210. A related configuration is that of fractures with two rough walls; dispersion is influenced in addition in this case by local aperture variations and inertial effects (for $Re > 1$) so that the variation of D with Pe may be more complex [11].

The same Taylor mechanism is also dominant in periodic $2D$ or $3D$ porous media [24,25] such as ordered $3D$ sphere packings [26] or periodic networks of channels [6] but only for flow parallel to a crystallographic axis. In this case, the stream tubes are periodic while, as for Taylor dispersion, solute can only move across streamlines through molecular diffusion. Due to the periodicity of the lattice in the directions transverse to the flow, the local flow field is the same as in a single channel of varying cross section parallel to the mean flow and with periodic boundary conditions on the sides: the resulting dispersion coefficient is then proportional to Pe^2.

The present work deals only with disorder at the pore scale and with short correlation lengths: in the models which are studied, dispersion results therefore solely from a combination of the geometrical and Taylor mechanisms. The effects of large scale heterogeneities or of a broad distribution of pore sizes have not been studied.

2 Description of experiments and data analysis

2.1 Experimental set-up and procedure

The experimental models used here closely resemble that used by Baudet and coworkers [27]. In this latter work, solute dispersion was measured in a long capillary tube filled with monodisperse beads and with a tube/bead diameter ratio $a/d \simeq 1.25$. The layout of the beads was either periodic or disordered. The first configuration was achieved by adding one by one beads in an horizontal capillary tube. Finally, one ends up with a line of beads, each of them being in contact with its two neighbors and with the tube wall. The second layout is obtained by tilting the capillary tubes while filling them. The beads fall then on top of each other and slide often sideways, resulting in a denser packing. The final packing is random and beads are added in the tube until it is entirely filled.

In this work, the inner diameter of the capillary tube is $a = 3.1 \pm 0.1$ mm, its length is 1500 mm and well calibrated stainless steel spheres of diameter $d = 2.54 \pm 0.02$ mm are used. In addition to these two bead packs, two more configurations were used (see Fig. 1). The first one uses the same tube but empty. In the last one, the diameter of the beads is $d = 1 \pm 0.01$ mm, i.e. three time smaller than the tube diameter, leading to a larger tube-to-particle ratio. In order to clarify the present paper, the following convention is used:

- (E) *Empty channel*: the capillary tube does not contain any beads ($a = 3.1$ mm).
- (O) *Ordered channel*: the tube contains a periodic line of beads touching each other ($a/d = 1.22$).
- (DI) *Disordered channel I*: the beads are still touching each other but build up a disordered array ($a/d = 1.22$).

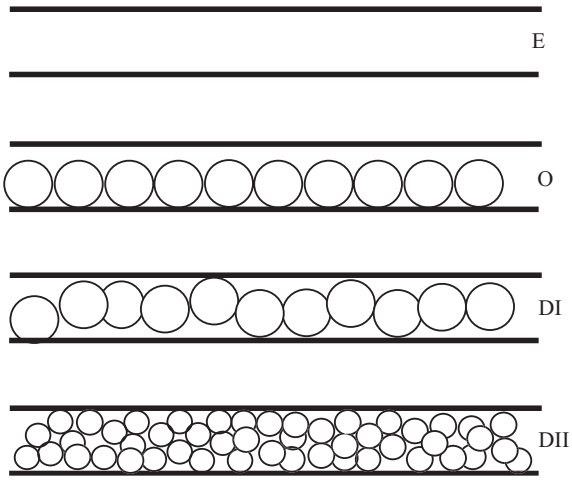

Fig. 1. Flow geometries used in the experiments. From top to bottom: Empty Channel - Ordered Channel - Disordered Channel I - Disordered Channel II.

– (*DII*) *Disordered channel II*: the arrangement is of the same type as (*DI*) but the diameter of the beads is smaller with $d = 1 \pm 0.01$ mm. ($a/d = 3.1$).

In configurations (O) and (DI), the diameter of the spheres is slightly smaller than the tube diameter ($d = 2.54 \pm 0.02$ mm). In configuration (*DII*), the diameter of the beads is three times smaller than that of the tube ($d = 1 \pm 0.01$ mm).

Originally, one end of the capillary tube is connected to a syringe pump allowing to establish a stationary flow of the transparent fluid through the channel: A valve allows to switch the injection to a dyed solution of identical properties. Fluid flowing out of the other end of the tube is weighed by computer controlled scales, allowing to measure the flow rate throughout the experiment.

The fluids used are solutions of either 10% or 70% of glycerol in water and their dynamic viscosities μ are respectively 1.3 mPa.s and 23 mPa.s (at 20 °C). Water Blue dye at a concentration of 0.05 g/l is added to one of the solutions: It has been selected because it is chemically stable and does not modify the rheological properties of the solution. The molecular diffusion coefficient D_m of the dye was determined through independent Taylor dispersion measurements performed in a vertical teflon capillary tube. One obtains in this way $D_m = 6.5 \times 10^{-4}$ mm^2/s for the 10% glycerol solution; for the 70% solution, the value $D_m = 3.25 \times 10^{-5}$ mm^2/s is deduced from the value for the first solution by the Stokes-Einstein relation [28].

In the following, the mean flow velocity U is characterized by the Péclet number Pe defined by taking $\ell = a$ in equation (2) for configurations (O), (DI) and (E) ($Pe = Ua/D_m$) and $\ell = d$ ($Pe = Ud/D_m$) in configuration (DII). In the present experiments, Pe ranges from 50 to 10^4 for the 10% glycerol solution but reaches 1.4×10^5 for 70% glycerol solutions. In all the studies the Reynolds number is less than 10: Under such conditions, the flow can be considered as stationary [12].

In this work, the variation of the solute concentration at the outlet with time, known as the breakthrough curve, is determined from light absorption by the dye. The measurement is realized over a square window of size 0.3 mm^2 located at 1450 mm from the injection, close to the outlet and immediately downstream of the last bead of the bed. In order to reduce optical distorsion induced by the tube curvature, the measurement section is enclosed within a transparent plexiglas cell with flat parallel walls. The cell is originally filled with glycerol, a fluid with a refractive index close to that of the tube. The section of the tube inside this cell is inserted between a light panel and a 4096 gray levels CCD camera (Roper Coolsnap CF). The set-up is illuminated by a fluorescent tube placed on the opposite side from the camera and excited at a high frequency to reduce fluctuations.

For each experiment, 2000 images are recorded by a computer connected to the camera at time intervals ranging from 1 to 30 s depending on the flow rate. Dye concentration values are determined quantitatively using calibration measurements realized independently with the experimental tube saturated with dye solutions of different known concentrations. Finally, drifts of the light intensity are measured in a region of interest outside the tube; these measurements are then used during the analysis of the images to compensate for the effect of these variations on the transmitted light intensity in the experimental section.

Using this experimental procedure, breakthrough curves were measured for different flow velocities and for different bead layouts. The results of these global measurements are given and discussed in Section 3. Moreover, in order to improve interpretations of the breakthrough curves, visualizations were realized independently at a local scale in a similar configuration. In these latter experiments, a transparent tube of $a = 8$ mm inner diameter is filled with glass beads of diameters 6, 3 or 2 mm. These beads were chosen so that the corresponding tube/bead diameter ratio is respectively 1.33, 2.67 and 4, close to the values used in the dispersion experiment. Originally, the model is saturated with glycerol (viscosity $\simeq$1 Pa.s) which is displaced by the same fluid but dyed. Using a fluid with such a high viscosity (and therefore a low diffusion coefficient) allows one to observe and separate clearly the various flow paths at low Reynolds numbers inside the sample.

Before describing in detail the various dispersive regimes observed for the different bead layouts, the next section describes the methods used to determine the dispersion coefficients from the breakthrough curves.

2.2 Analysis of the experimental curves

Figure 2 displays a typical breakthrough curve obtained after a stepwise injection of the dyed fluid; asymmetrical curves were also obtained and their analysis will be discussed later. Under such initial conditions, and if the concentration satisfies the classical convection-diffusion equation given by equation (1), the concentration variation at

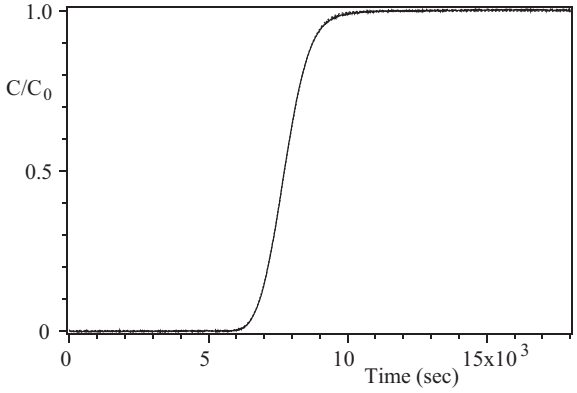

Fig. 2. Continuous line: typical dye concentration variation as a function of time for a type $DI-$ array and for $Pe = 930$ (continuous line). Dotted line: curve fitted with a variation from equation (6). The experimental and fitted curves almost completely coincide but for a small separation in the top center of the figure.

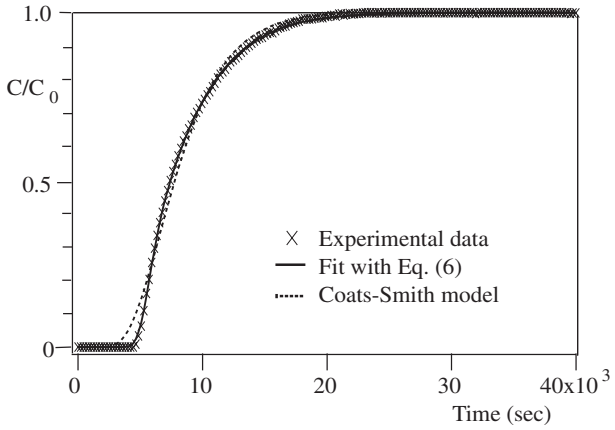

Fig. 3. (×): experimental dye concentration variation as a function of time for an ordered $O-$type array of 2.54 mm diameter beads and for $Pe = 1000$. Dotted (resp. continuous) lines: Gaussian (resp. Coats-Smith) fits.

the outlet is given by:

$$\frac{C(L,t)}{C_0} = \frac{1}{2}(1 - erf\frac{L - Ut}{\sqrt{4D\ t}}). \qquad (6)$$

Where, C_0 is the dye concentration in the displacing fluid, L the distance between the measurement section and the injection point, D is the longitudinal dispersion coefficient, U is the mean flow velocity. Figure (2) shows the fit of the breakthrough curve by the function given by equation (6) where the only adjustable parameter is D. The two curves are almost undistinguishable, indicating that the dispersion process is Fickian and that the classical convection-diffusion equation (1) is satisfied.

This good agreement was to be expected for the disordered models. The tube length represents at least 600 bead diameters (for the largest beads) and is therefore much larger than the correlation length of the velocity field which is of a few bead diameters: the conditions for obtaining a diffusive spreading are therefore met. For the empty tube (E), the correlation length of the velocity field is equal to the tube length: the classical condition for reaching a Gaussian Taylor dispersion regime is that the mean transit time τ_t along the tube must be larger than the transverse diffusion time. These issues have been studied in detail by several authors [13,14] and a usual practical condition is $\tau_t \gg a^2/16D_m$ in which a is the diameter. In the present case, this leads to $\tau_t > 1000$ s. This condition is fulfilled in the present experiments for which the minimum transit time is of the order of 5000 s. Yet, in the (O) configuration and for fairly high velocities U, one observes at long times (as can be seen in Fig. 3) a "tail" effect and equation (1) is no more verified. This results from the large diffusive exchange time between the slow and fast part of the flow sections which is not short enough compared to the transit time along the sample (see Sect. 3.2).

In this case, the experimental breakthrough curves are well fitted by solutions of the classical Coats-Smith capacitive model [29]: it assumes zero flow regions (representing a fraction $1-f$ of the total volume exchanging solute with flowing zones (fraction f of the volume) through an exponential process with a characteristic exchange time T_f. The model uses 4 fitting parameters: f, T_f, the mean velocity U and a parameter D_f characterizing dispersion in the flowing regions. Let us call x the distance from the inlet at which the concentration variation is measured: if the medium does not display large scale heterogeneities with a characteristic size of the order of or larger than x, then the fitting parameters are independent of x. If this distance x is such that $\overline{t} \leq T_f$, the concentration variation curves display a long time "tail" with a characteristic relaxation time directly related to T_f and the curves cannot be fitted by variations from equation (6). At long distances such that $\overline{t} \gg T_f$, on the contrary, the concentration variation curves are well fitted by using equation (6) and the corresponding "asymptotic" dispersion coefficient D_{as} can be shown to satisfy the relation [29,30]:

$$\frac{D_{as}}{D_m} = \frac{D}{D_m} + (1-f)^2\frac{U^2 T_f}{D_m}, \qquad (7)$$

The Coats-Smith procedure is valid because the (O) configuration is periodic and no additional heterogeneity is added if the length is increased, D_{as} represents then the value of the dispersion coefficient that would be measured for a model of larger length containing an identical periodic array of the same beads. In the following, the dispersivity l_d is taken equal to D_{as}/U only for experiments in the (O) configuration. In the other configurations, D is obtained simply by fitting the experimental curves to equation (6).

3 Experimental results

Figure 4 displays variations of the dispersivity l_d as a function of the Péclet number measured for the different channel configurations used in the present work. Note that all

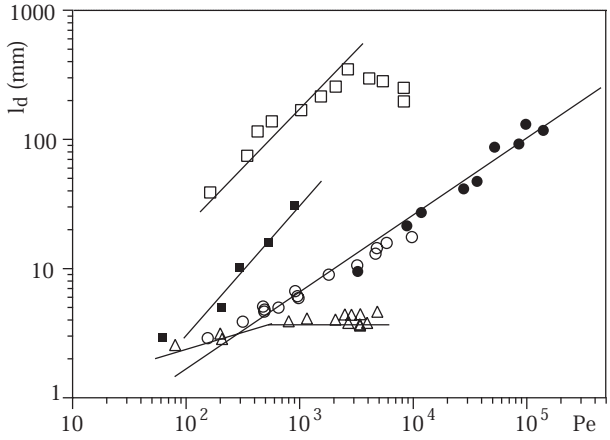

Fig. 4. Variation of the dispersivity l_d as a function of the Péclet number: ($\triangle$) $DII-$array; ($\circ, \bullet$) $DI-$ array respectively for solutions of 10% and 70% glycerol in water; ($\blacksquare$) $E-$ channel; ($\square$) $O-$ channel (in this latter case $l_d = D_{as}/U$).

the experiments were carried out twice: first, the dyed fluid was injected to displace the clear solution flowing initially in the model at the same flow rate. After the model has been completely saturated with the dyed fluid, it is displaced in a second experiment by the clear fluid, still at the same flow rate. The dispersion coefficient was found to be identical in the two experiments, implying that no instabilities modified the flow.

3.1 Empty tube (E-Channel)

In the case of an empty tube, all the experimental dispersion curves are well adjusted by the concentration variation given by equation (6). The corresponding dispersivities l_d are plotted in Figure 4 in log-log coordinates: for $Pe \geq 100$, the data points ($\blacksquare$) fall on a straight line of slope 1, indicating that $l_d \propto Pe$. This is in agreement with equation (5) which predicts, in this range of Péclet numbers, a linear variation of l_d with Pe (the linear term is at least 50 times larger than the Pe^{-1} one). Using a linear regression on the experimental values of l_d, equation (5) provides an estimation of the tube diameter: $a_{eff} \simeq 3 \pm 0.2$ mm. This effective value coincides very well with the actual diameter of the tube (3.1 ± 0.1 mm) which confirms (as expected) that Taylor dispersion is the dominant mechanism in the empty tube.

3.2 Ordered array of beads (O-Channel)

Dispersivity l_d values obtained for the ordered array of beads by means of the Coats-Smith model are plotted in Figure 4. For $Pe \leq 2500$, l_d varies with Pe following a power law : $l_d \sim a_{eff} Pe^{\gamma}$ (straight line in log-log coordinates). From a regression over the experimental data, one obtains $a_{eff} \simeq 0.6$ mm and $\gamma = 0.85 \pm 0.2$: this value is compatible with a Taylor dispersion mechanism for which $\gamma = 1$ (as above, the Pe^{-1} term in Eq. (5) is negligible). It

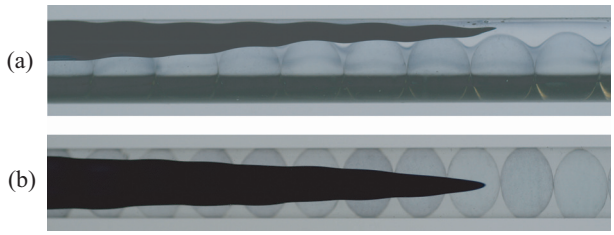

Fig. 5. Miscible displacement of pure by dyed glycerol in an ordered array of beads inside a capillary tube: (a) side view (b) top view (bead diameter: $d = 6$ mm; tube diameter: $a = 8$ mm).

is to be noted that the value of a_{eff} is of the order of the distance between the top of the beads and the upper tube wall: this distance represents an effective aperture for the Taylor process, possibly because the transverse diffusion time which control the dispersivity value is lower in the regions where the flow section is smallest.

These results agree therefore with the expectations that, in this channel, fluid particles follow periodic streamlines determined by the structure of the bead packing: as in the capillary tubes, the molecules of dye can only explore the section of the flow channel through molecular diffusion resulting from Brownian motion (see Fig. 5).

An important feature is the fact that the experimental values of l_d which vary from 40 mm to 400 mm are about 8 times larger than for the empty capillary tube at a same mean flow velocity. This cannot be explained by the partial filling up of the flow channel by the beads. On the opposite, since these reduce the effective aperture of the flow channels, l_d should drop off following equation (5) which is not observed.

Globally, the values obtained are in qualitative agreement with reference [24] which predicts an enhancement of dispersion with a large Taylor-like component in $3D$ periodic media for flow parallel to a crystal axis; similar results have also been reported in other works on periodic $2D$ and $3D$ systems [6,25].

Direct visualizations realized in a similar periodic geometry (Fig. 5), but with larger beads, complement usefully these results: pure glycerol is used to visualize clearly the boundaries between fluids by removing the influence of molecular diffusion.

In this figure, one observes that the dyed fluid displays a tongue like structure and wraps around the beads. This shape shows that the streamlines are mostly oriented in the flow direction with tiny undulations induced by the beads. Two very important points are that no splitting of the displacement front is observed and that the dyed fluid does not flow at early times into the narrow space between the beads: mass transfer between the two regions thus only occurs through molecular diffusion which explains the "tail" observed in the breakthrough curves at high flow velocities. Finally, the tongue-like structure reveals the strong velocity contrast between the fluid flow on the side of the beads and above them. The velocity gradient stretches the front of dye resulting in a concentration

gradient which, in turn, gets smoothed by a transverse diffusive flux.

All ingredients of a Taylor like dispersion regime are thus present. Yet, because of the beads, the diffusive flux path is more tortuous than in an empty capillary tube: solute has to flow around the beads to reach the outlet of the tube. The time needed to homogenize the dye concentration in the tube section is thus longer, resulting in a higher dispersivity; also, dye needs to diffuse across the full diameter of the tube (from the bottom to the top channel) rather than only across the radius as in the empty tube so that the characteristic diffusion time is four times larger.

At the highest flow velocities, the variation of l_d levels off and starts to decrease. A possible explanation is the fact that, in this range of Pe values, the Reynolds number becomes higher than 1 ($Re > 5$): recirculation and/or secondary flows may then develop and induce a more efficient transverse mixing than molecular diffusion. This will shorten the transverse exchange and this new value should replace the characteristic transverse molecular diffusion time a^2/D_m in the computation leading to equation (5). The dispersivity l_d would therefore be reduced at high Pe values as observed experimentally.

3.3 Disordered array of small beads (DII-array)

For a disordered array of 1 mm diameter beads inside the tube, the dispersivity l_d increases slowly as a function of Pe before reaching a constant value of the order of 3 mm for $Pe \gtrsim 600$. This constant limiting value of l_d implies that geometrical dispersion associated with the random velocity variations from one pore to the next is dominant. This is not surprising since, in such geometries, the correlation length of the velocities of fluid particles along their path is too short for Taylor dispersion to develop. Dispersion characteristics of such arrays are then comparable to those of non homogeneous nonconsolidated packings of monodisperse grains [16,31]: in this latter case, the value of l_d for Péclet numbers (based on the grain size) of the order of 1000 is $\simeq 2d$. In Figure 4, the value of l_d for a similar Péclet number ($Pe = 3000$ when based on the tube diameter) is $l_d = 3$ mm or about three times the bead diameter i.e. only 50% higher. The variations of l_d with Pe are qualitatively also very similar in both cases with a slow increase up to $Pe \simeq 1000$ and a constant value at higher velocities.

Visualizations realized with $d = 2$ and 3 mm beads inside a tube of diameter $a = 8$ mm (Figs. 6a–b) complement these results. Figure 6a demonstrates clearly the many divisions of the front of injected fluid after moving through several pores and the rather uniform distribution of the invading fluid across the flow section: for the less viscous fluids used in our dispersion experiments, transverse molecular diffusion would mix quickly these thin filaments with the surrounding fluid, leading to the Gaussian dispersion observed for the $DII-$ array. In samples with such small a/d ratios, some wall effects and perturbations of the packing structure are probably present [32]: they likely account for the 50% increase of the values of l_d/d compared

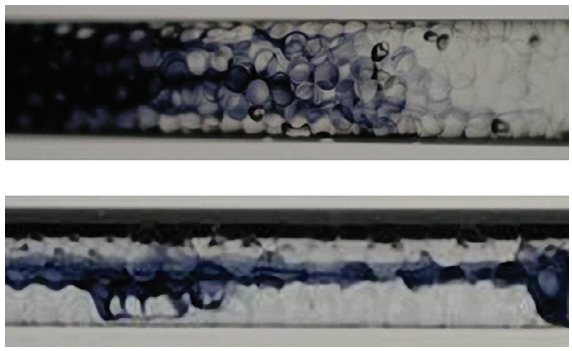

Fig. 6. Miscible displacements of pure glycerol by dyed glycerol saturating disordered glass beads packings inside a $a = 8$ mm diameter capillary tube. Bead diameter: (a) $d = 2$ mm – (b) $d = 3$ mm. The tube/particle diameter ratio is respectively 4 and 2.66.

to those reported in reference [16] for much larger a/d values. However, from this relatively small variation of l_d/d together with the fact that no clear preferential flow is visible near the tube walls, we can conclude that confinement effects do not influence crucially the dispersion process.

Another potential problem is the appearance of a local order of the monodisperse beads in sample DII. The circular geometry is not favourable, particularly for such a low a/d ratio since the beads would build up hexagonal or cubic lattices. It is however possible that, for some values of the ratio a/d pathological features of the structure appear: this is for instance the case in the packing shown in Figure 6b and corresponding to $a/D = 2.66$ in which flow is strongly channelized in the center of the column. Such a flow structure would give rise to early first arrival times in the dispersion curves and is also easily detectable in the visualizations. No such effects are visible either in the picture of Figure 6a or in the concentration variation curves observed for sample (DII). One concludes therefore that packings with carefully chosen low values of the ratio a/d may display dispersion characteristics quite similar to those obtained for much larger values of a/d.

3.4 Disordered array of large beads (DI-array)

In this case (see Fig. 1), the beads have the same diameter as in the periodic $O-$ channel (i.e. $d = 2.54$ mm), but the packing is now weakly disordered (ie the beads are slightly displaced laterally at random from the location they would have in a periodic row). The experiments were performed using the two water-glycerol solutions containing either 10% or 70% of glycerol in weight. As for the DII array and in contrast with the ordered one, all breakthrough curves are well adjusted by equation (6) allowing for the determination of D for the various flow conditions. The Figure 4 shows the dispersivity $l_d = D/U$ as a function of the Péclet number for the two solutions used in the experiments.

Clearly, the dispersivity l_d and Pe have a power law relationship. Fitting the variation of l_d with Pe to $a_{eff} Pe^{\gamma}$ gives respectively for the 10% and 70% glycerol solutions

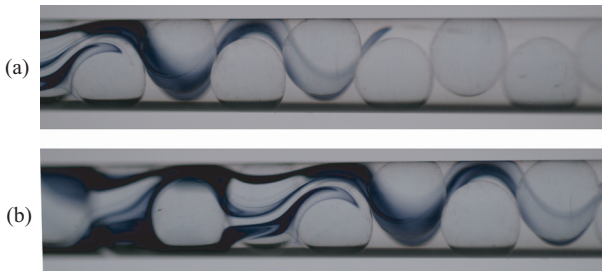

Fig. 7. Views at different times of the miscible displacement front of pure by dyed glycerol in a disordered channel: the diameter of the beads is $d = 6$ mm and the diameter of the tube $a = 8$ mm. The tube-to-particle ratio is 1.33.

$\gamma = 0.52 \pm 0.01$, $a_{eff} \simeq 0.2$ mm and $\gamma = 0.69 \pm 0.04$, $a_{eff} \simeq 0.04$ mm. One observes that a_{eff} and γ are only slightly different for the two solutions despite a ratio of 20 between the viscosities. One notices that the values of l_d for a given Péclet number are much lower for the disordered array than for the periodic one (by a factor of 15 (resp. 40) at low (resp. high) Pe values) although the bead and tube diameters are identical. Also, at low Péclet numbers, l_d becomes of the order of the bead size and gets close to the dispersivity observed for the DII array.

An important feature is the fact that the exponent γ characterizing the variation of l_d with Pe is of the order of 0.5 (for the 10% solution) and of 0.69 for the other solution (at slightly higher Péclet numbers). These exponents are intermediate between the values 0.82 ± 0.2 for the periodic array and 1 for the empty tube and the value 0 (constant l_d) for the disordered packing of smaller beads: This implies that the dispersion mechanism is intermediate between Taylor and geometrical dispersion corresponding respectively to the first and second cases. This result was also observed by Baudet et al. [27] but remained unexplained.

As in the previous sections, visualizations on a larger system with the same d/D ratio help understand the dispersion mechanisms. The visualizations of Figure 7a–b show that the dyed fluid is mostly split into two streaks located near the walls. This localization likely reflects an increase of the porosity near the walls [32]; moreover, the low value of the tube/bead diameter ratio (of the order of 1) breaks the angular isotropy of the porous structure and concentrates the flow paths in a few (here 2) channels. Magnico [15] estimated that, at low Reynolds numbers, a fluid layer of thickness of the order of $d/4$ appears, inside which fluid flow is purely longitudinal and tangential with no radial component. At first, one expects therefore radial exchange between the dye streaks, clearly visible on Figure 7a, and the remaining pore space to be mostly diffusional. Yet, as can be seen in Figure 7b, structural heterogeneity resulting from displaced beads splits the streaks into filaments parallel to the mean flow [12]; the number of filaments increases then along the flow path and their size decreases. These filaments persist over distances significantly larger than the bead diameter so that molecular diffusion may spread the filaments over transverse distances of the order of their size. This gives rise to Taylor-like dispersion so that the global dispersion results from the combined influences of geometrical and Taylor dispersions. Such an influence of the flow channelization on dispersion was recently reported by Bruderer et al. [6] in $2D$ networks.

3.5 Qualitative model of different power law variations

A qualitative argument helps understand how one can reach such power law variations of $l_d \propto Pe^{\gamma}$ $(0 < \gamma < 1)$ under the combined influence of the disorder of the flow field and of transverse molecular diffusion. Assume that the front gets divided into streaks of width a_x decreasing with the distance x parallel to the flow as $a_x \sim d^{1+\beta}x^{-\beta}$ (the d term allows to have the right dimensionality for the equation). By generalizing the Taylor argument, the transition to diffusive spreading should occur when the transverse molecular diffusion time τ_{diff} across the distance a_x is of the order of the mean transit time L/U with:

$$\tau_{diff} \sim \frac{a_x^2}{D_m} \sim \frac{x}{U}. \tag{8}$$

Replacing a_x by its expression provides the distance at which the transition should take place:

$$x_{trans} \sim d(\frac{Ud}{D_m})^{1/(1+2\beta)} \sim dPe^{1/(1+2\beta)}. \tag{9}$$

With, as usual, $Pe = Ud/D_m$. As in Taylor dispersion, x_{trans}, represents the characteristic decorrelation distance of the velocity of solute particles and we assume therefore that $D \sim Ux_{trans}$ leading to

$$D_{eff} \sim UdPe^{1/(1+2\beta)} \tag{10}$$

or

$$\frac{D_{eff}}{D_m} \sim Pe^{\frac{2+2\beta}{1+2\beta}}. \tag{11}$$

For $\beta = 0$ (no geometrical variation of the width of the filament with distance), one retrieves Taylor dispersion with $D_{Taylor} \sim a^2U^2/D_m$ and, for $\beta = \infty$ (fast decorrelation), one obtains geometrical dispersion with $D_{geom} \sim dU$ (the exponent γ defined previously should then be related to β by $\gamma = 1/(1 + 2\beta)$). In the present case, the experimental result $D \propto Pe^{3/2}$ implies that $\beta = 1/2$. Therefore, the experimental observations on $DI-$ may be accounted for by assuming a combination of the influences of transverse molecular diffusion and of the geometrical disorder of the packing with, for the latter, a rate of division of the dye streaks intermediate between those observed in a packing of small beads and in a capillary tube.

4 Conclusion

To conclude, despite its simple structure (a long tube filled up with beads), the experimental system studied

in the present work displays a broad variety of dispersion regimes. While wall effects control the classical Taylor dispersion in the empty tube, the structure and geometry of the bead packings filling the tube play a dominant part in all other cases. More specifically, both the degree of disorder of the layout of the beads and the ratio of their diameter to that of the tube are observed to influence the dispersion characteristics.

The results obtained may be particularly useful to understand flow and solute transport in such systems as fractures with rough walls, networks of flow channels in microfluidic applications, flow devices used in hydrodynamic separation or periodic or near periodic porous media. One observes for instance dispersivity variations with intermediate power laws similar to those presented here in weakly disordered $2D$ networks of channels [7].

First, Taylor dispersion has been observed for a periodic bead array inside a tube of slightly larger diameter than the beads, like in the empty tube but with a significantly increased dispersion coefficient. With the same beads inside the same tube, but packed in a weakly disordered array, the dispersivity l_d is strongly reduced and the exponent γ characterizing the variation of l_d with Pe decreases from almost 1 to 0.5. This variation reflects the reduced persistence length of solute streaks due to their getting repeatedly split as they move along the tube (this length remains however much larger than the bead diameter). A simple model assuming a power law reduction of the width of the streaks of dye with distance allows to reproduce this variation of l_d with Pe. When the ratio of the tube and particle diameters is increased by using beads of smaller diameter, the dispersion coefficient varies with the Péclet number as $D \propto Pe$ for $Pe > 600$. This reflects a geometrical dispersion regime with a still shorter persistence length of the dye streaks reflecting a correlation length of the flow field of the order of the bead size.

More observations of the flow and concentration fields at the local scale (using for instance matched index fluids) are needed to explain *quantitatively* these results. The increase of the dispersivity for the periodic array compared to the empty tube and the decorrelation of the motions of the fluid particles in the disordered arrays for small tube/particle diameter ratios are two particularly important issues.

We thank J. Koplik and G. Drazer for very helpful comments and discussions. This work was supported by UBA-$IN029$, by the CNRS-Conicet International Cooperation Program (PICS N° 2178) and by the ECOS Sud program N° $A03E02$.

References

1. J. Bear, *Dynamics of Fluids in Porous Media* (Dover Publications, New York, 1988)
2. F.A.L. Dullien, *Porous media, fluid transport and pore structure*, 2nd ed. (Academic Press, New-York, 1991)
3. *Flow and Contaminant Transport in Fractured Rock*, edited by J. Bear, C.-F. Tsang, G. de Marsily (Academic Press, New-York, 1993)
4. M. Sahimi, *Flow and Transport in Porous Media and Fractured Rocks: From Classical Methods to Modern Approaches* (John Wiley and Sons, New-York, 2005)
5. J.C. Bacri, J.P. Bouchaud, A. Georges, E. Guyon, J.P. Hulin, N. Rakotomalala, D. Salin, *Hydrodynamics of dispersed media*, edited by J.P. Hulin, A.M. Cazabat, E. Guyon, F. Carmona (North Holland, Amsterdam, 1990) pp. 249–269
6. C. Bruderer, Y. Bernabé, Water Resour. Res. **37**, 897 (2001)
7. M.V. D'Angelo, H. Auradou, C. Allain, J.-P. Hulin, Phys. Fluids **19**, 033103 (2007)
8. D.G. Dronfield, S.E. Silliman, Water Resour. Res. **29**, 3477 (1993)
9. I. Ippolito, G. Daccord, E.J. Hinch, J.P. Hulin, J. Contamin. Hydrol. **16**, 87 (1994)
10. R.L. Detwiler, H. Rajaram, R.J. Glass, Water. Resour. Res. **36**, 1611 (2000)
11. A. Boschan, H. Auradou, I. Ippolito, R. Chertcoff, J.P. Hulin, Water Resour. Res. **43** W03438 (2007)
12. T.H. Wegner, A.J. Karabelas, T.J. Hanratty, Chem. Eng. Sci. **26**, 59 (1971)
13. P.C. Chatwin, J. Fluid Mech. **43**, 321 (1970)
14. M.J.E. Golay, J.G. Atwood, J. Chromatogr. **186**, 353 (1979)
15. P. Magnico, Chem. Eng. Sci. **58**, 5005 (2003)
16. J.J. Fried, M.A. Combarnous, Adv. Hydrosci. **7**, 169 (1971)
17. P.G. Saffman, J. Fluid Mech. **6**, 321 (1959)
18. P.G. Saffman, J. Fluid Mech. **7**, 194 (1960)
19. D.L. Koch, J.F. Brady, J. Fluid Mech. **154**, 399 (1985)
20. C. Baudet, E. Guyon, Y. Pomeau, J. Phys. Lett. **46**, L-991 (1985)
21. J. Koplik, *Disorder and Mixing*, edited by E. Guyon, Y. Pomeau, J.P. Nadal (Kluwer, Dordrecht, the Netherlands, 1988) pp. 123–137
22. G.I. Taylor, Proc. Roy. Soc. London A **219**, 186 (1953)
23. R. Aris, Proc. Roy. Soc. London A **235**, 67 (1956)
24. D.L. Koch, R.G. Cox, H. Brenner, J.F. Brady, J. Fluid Mech. **200**, 173 (1989)
25. J. Salles, J.-F. Thovert, R. Delannay, L. Prevors, J.-L. Auriault, P.M. Adler, Phys. Fluids A **5**, 2348 (1993)
26. R.S. Maier, D.M. Kroll, R.S. Bernard, S.E. Howington, J.F. Peters, H.T. Davis, Phys. Fluids **12**, 2065 (2000)
27. C. Baudet, R. Chertcoff, J-P. Hulin, C.R. Acad. Sci. Paris, II **305**, 429 (1987)
28. W.B. Russel, D.A. Saville, W.R. Schowalter, *Colloidal Dispersions* (Cambridge University Press, Cambridge, UK, 1995), Chap. 3
29. K.H. Coats, B.D. Smith, Soc. Pet. Eng. J. Trans. AIME **231**, 73 (1964)
30. J. Villermaux in *Percolation processes, theory and applications*, edited by A. Rodrigues, D. Tondeur (Kluwer, Dordrecht, 1981), pp. 83–140
31. N-W. Han, J. Bhakta, R.G. Carbonell, AIChE **31**, 277 (1985)
32. G.E. Mueller, Powder Technol. **72**, 269 (1992)